Proton-Proton Bremsstrahlung Including Rescattering*

VIRGINIA R. BROWN
Lawrence Radiation Laboratory, University of California, Livermore, California 94550
(Received 9 September 1968)

The theory of proton-proton bremsstrahlung treating the nuclear interaction exactly and the electromagnetic interaction to first order is formulated so as to include the exact determination of the rescattering term. The effect of the Coulomb interaction between the two protons is not considered. The off-energy-shell nuclear matrix elements are written so as to eliminate the necessity of integrating over the nuclear potential. Coplanar symmetric cross sections are calculated with the one-boson-exchange momentum-dependent potential of Bryan and Scott and the hard-core potential of Hamada and Johnston, including partial-wave contributions of the nuclear matrix elements with $J \leq 4$. All results include rescattering corrections, which are shown by explicit calculation to be small ($\leq 15\%$). Quantitative agreement with existing experiments, including the characteristic quadrupole photon angular distribution, is obtained. Present experiments are inadequate to differentiate definitively between the Hamada-Johnston hard-core potential and the Bryan-Scott momentum-dependent potential.

I. INTRODUCTION

THE theoretical aspects of proton-proton bremsstrahlung were originally treated by Ashkin and Marshak[1]; interest in the problem as applied to the study of the off-energy-shell behavior of various nucleon-nucleon potentials has received a revitalization, both experimentally and theoretically, with the work of Sobel and Cromer.[2] A number of experiments,[3–13] as well as several calculations,[14–20] have followed.

The present study constitutes an elaboration and extension of an earlier paper,[18] hereafter referred to as A. Presented in A were the first p-p-γ results using a realistic potential for which quantitative agreement with existing experiments, including the characteristic photon angular distribution, was obtained. At the time of publication of A, however, there were both quantitative and qualitative disagreements with the calculations of Cromer and Sobel[14] and with those of Marker and Signell.[21] The results of A at 46 MeV were a factor of the order of 6 lower than either the results of Cromer and Sobel or those of Marker and Signell, and this disagreement increased with decreasing energy. An important qualitative disagreement was in the photon angular distribution. The results of A showed a quadrupole angular distribution, while both the results of Cromer and Sobel and those of Marker and Signell showed a dipole angular distribution. The results of A at 46 MeV were consistent with the experimental results of Warner[5] at 48 MeV and somewhat lower than those of Slaus *et al.*[6] at 46 MeV; they were close to, but higher than, the calculations of Pearce *et al.*[17] Experimental evidence for a quadrupole shape in the photon angular distribution at 46 MeV was not clearly demonstrated at that time. Since then, Mason *et al.*[9] have obtained a photon angular distribution at 47 MeV that is consistent with a quadrupole shape.

According to Signell,[22] and as discussed further by Drechsel and Maximon,[20] a substantial portion of these discrepancies is due to the neglect of the rescattering term when the effects of the electromagnetic potential are calculated in the laboratory frame with the use of a transverse gauge. In the present study, as in A, the calculation is done in the barycentric system, and the rescattering term, which is evaluated explicitly, is small. In addition, since the calculation is done entirely in the barycentric system, using invariance considerations to

* Work performed under the auspices of the U.S. Atomic Energy Commission.

[1] J. Ashkin and R. E. Marshak, Phys. Rev. **76,** 58 (1949); **76,** 989(E) (1949).
[2] M. I. Sobel and A. H. Cromer, Phys. Rev. **132,** 2698 (1963).
[3] B. Gottschalk, W. J. Schlaer, and K. H. Wang, Phys. Letters **16,** 294 (1965); Nucl. Phys. **75,** 549 (1966).
[4] B. Gottschalk, W. J. Schlaer, and K. H. Wang, Nucl. Phys. **A94,** 491 (1967).
[5] R. E. Warner, Phys. Letters **18,** 289 (1965); **19,** 719 (1965); Can. J. Phys. **44,** 1225 (1966).
[6] I. Slaus J. N. Verba, J. R. Richardson, R. F. Carlson, W. T. H. van Oers, and L. S. August, Phys. Rev. Letters **17,** 536 (1966).
[7] K. W. Rothe, P. F. M. Koehler, and E. H. Thorndike, Phys. Rev. Letters **16,** 1118 (1966); Phys. Rev. **157,** 1247 (1966).
[8] M. L. Halbert, D. L. Mason, and L. C. Northcliffe, Phys. Rev. **168,** 1130 (1968); and (private communication).
[9] D. L. Mason, M. L. Halbert, and L. C. Northcliffe, Phys. Rev. **176,** 1159 (1968).
[10] D. L. Mason, M. L. Halbert, A. van der Woude, and L. C. Northcliffe (unpublished).
[11] J. Thompson, S. Naqvi, and R. E. Warner, Phys. Rev. **156,** 1156 (1967).
[12] A. Bahnsen and R. L. Burman, Phys. Letters **26B,** 585 (1968).
[13] F. Sannes, J. Trischuk, and D. G. Stairs (unpublished).
[14] A. H. Cromer and M. I. Sobel, Phys. Rev. **152,** 1351 (1966); **158,** 1157 (1967).
[15] Y. Ueda, Phys. Rev. **145,** 1214 (1964).
[16] I. Duck and W. A. Pearce, Phys. Letters **21,** 669 (1966).
[17] W. A. Pearce, W. Gale, and I. Duck, Nucl. Phys. **B3,** 241 (1967).
[18] V. R. Brown, Phys. Letters **25B,** 506 (1967). An earlier account of this work was described in V. R. Brown, Bull. Am. Phys. Soc. **11,** 396 (1966); **12,** 471 (1967).
[19] P. Signell and D. Marker, Phys. Letters **26B,** 559 (1968).
[20] D. Drechsel and L. C. Maximon, Phys. Letters **26B,** 477 (1968).
[21] D. Marker and P. Signell (unpublished) (as quoted in Fig. 1 of Ref. 6).
[22] P. Signell, in *Proceedings of the International Conference on Light Nuclei, Few Body Problems, and Nuclear Forces, Brela, Yugoslavia, 1967* (Gordon and Breach, Science Publishers, Inc., New York, 1968).

obtain laboratory cross sections, the question of properly joining the amplitudes calculated with the electromagnetic matrix elements determined in the laboratory frame and the nuclear matrix elements determined necessarily in the two-nucleon c.m. frame does not arise.

The essential results here, as given in A, are that (a) a quadrupole shape is obtained for the angular distribution, which is suggested to be a model-independent feature[23]; (b) the rescattering corrections to the differential cross section are shown by explicit calculation to be small ($\leq 15\%$); (c) the method of evaluating the off-energy-shell nuclear matrix elements, though equivalent to previous methods, is simplified; and (d) present experiments are inadequate to differentiate definitively between the Hamada-Johnston[24] hard-core potential and the Bryan-Scott[25,26] momentum-dependent potential.

In view of the last result, the hope that p-p-γ might be sufficiently sensitive to the inner region of the nuclear interaction to distinguish between the various nucleon-nucleon potentials is somewhat diminished, at least for the accuracy with which the differential cross sections have been obtained thus far. The use of polarization effects, for which the rescattering-term contribution is important, as a possible method for exposing more of the off-energy-shell behavior of the two-nucleon potentials is presently being considered by the author.

In Secs. II–VI the formalism of p-p-γ, designed to include the exact determination of the rescattering contributions, is developed. It is intended that sufficient detail is included to avoid confusion, since a coherent treatment of p-p-γ without ambiguities and with rescattering is not available in the literature. The effect of the Coulomb interaction between the two protons is not considered in the present work. In Sec. II the T matrix for p-p-γ is expressed to first order in the electromagnetic interaction including the rescattering term, and is developed for use in the barycentric system. In Sec. III the effect of spin and polarization in the determination of the electromagnetic matrix elements is considered. The singlet-triplet spin representation is used for the p-p system, and the polarization states of the photon are treated in the circular basis, which corresponds to using a helicity representation for the photon. In Sec. IV the evaluation and interpretation of the off-energy-shell nuclear matrix elements are considerably simplified by expressing them in terms of volume and surface contributions, eliminating the necessity of integrating over the nuclear potential. The volume term goes to zero on the energy shell or in the limit of no photon emission, and the surface term which is evaluated beyond the range of the nuclear interaction is directly expressible in terms of the elastic phase shifts and scattering parameters. Presented in Sec. V is a method for evaluating the rescattering matrix elements, involving the partial-wave decomposition of the electromagnetic interaction. The cutoff in this partial-wave decomposition is provided by the cutoff in the partial-wave decomposition of the initial and final nuclear states, and is exhibited by the angular integration. The radial integration involves the evaluation of the product of three spherical Bessel and Neumann functions with limits from a point beyond the range of the nuclear interaction to infinity. Section VI contains the invariant form of the cross section suitable for the present study.

The results are presented in Sec. VII, where a comparison is made between the hard-core potential of Hamada and Johnston[24] and the momentum-dependent potential of Bryan and Scott.[25,26] These results include higher partial-wave contributions and wider angular dependence and energy range than those presented in A. In particular, the present work includes partial-wave contributions from the nuclear matrix elements with $J \leq 4$, as well as cross sections for coplanar symmetric angles from 20° to 40° with an incident laboratory energy ranging from 10 to 300 MeV. Also included is a partial-wave analysis of the results at 158 MeV with coplanar symmetric angles of 30° for the Hamada-Johnston potential. These results demonstrate the importance of the off-diagonal matrix elements in the evaluation of p-p-γ cross sections at this energy, and correspondingly suggest the necessity of using a potential for which the effects of the tensor force are considered. The explicit behavior of the rescattering contribution as a function of the photon angular distribution for the Hamada-Johnston potential is also presented at 158 MeV with coplanar symmetric angles of 30°.

II. T-MATRIX FORMULATION; BARYCENTRIC SYSTEM

The Hamiltonian for p-p-γ can be written

$$H = K_1 + K_2 + K_\gamma + V_{\rm em} + V_N, \qquad (2.1)$$

where K_1 and K_2 represent the kinetic energies of the two protons, K_γ is the free-field Hamiltonian of the quantized electromagnetic field, V_N is the nuclear potential, and $V_{\rm em}$ is the electromagnetic interaction. The two-potential expansion[27] of the complete T matrix

[23] E. M. Nyman, Phys. Letters **25B**, 135 (1967); Phys. Rev. **170**, 1628 (1968).

[24] T. Hamada and I. D. Johnston, Nucl. Phys. **34**, 382 (1962).

[25] R. A. Bryan and B. L. Scott, Phys. Rev. **164**, 1215 (1967); and (unpublished).

[26] The potential used in the present calculation is a modification of that given in Ref. 25. The modification consists of new input parameters and the use of a cutoff factor in order to give an S-as well as a higher partial-wave fit. The new parameters used here are, in the notation of Ref. 25, $g_\pi^2 = 12.5$, $g_{\sigma_1}^2 = 1.65$, $m_{\sigma_1} = 600$ MeV, $g_\rho^2 = 1.81$, $f_\rho/g_\rho = 1.13$, $g_\eta^2 = 2.60$, $g_{\sigma_0}^2 = 8.19$, $m_{\sigma_0} = 550$ MeV, $g_\omega^2 = 17.3$, and $f_\omega/g_\omega = 0$. The cutoff is introduced in momentum space through a Feynman factor $\Lambda^2/(\Lambda^2+q^2)$, where $\mathbf{q}$ is the momentum transfer and with $\Lambda = 1500$ MeV.

[27] B. Lippmann, Ann. Phys. (N.Y.) **1**, 113 (1957).

to first order in the electromagnetic interaction yields[28]

$$T_{fi}=\langle \mathbf{p}_{1f}\mathbf{p}_{2f} \mid V_{\rm em}G_0(E_i)T_N(E_i) \mid \mathbf{p}_{1i}\mathbf{p}_{2i}\rangle + \langle \mathbf{p}_{1f}\mathbf{p}_{2f} \mid T_N^{\ddagger}(E_f)G_0(E_f)V_{\rm em} \mid \mathbf{p}_{1i}\mathbf{p}_{2i}\rangle + \langle \mathbf{p}_{1f}\mathbf{p}_{2f} \mid T_N^{\ddagger}(E_f)G_0(E_f)V_{\rm em}G_0(E_i)T_N(E_i) \mid \mathbf{p}_{1i}\mathbf{p}_{2i}\rangle, \quad (2.2)$$

where the initial and final proton free-scattering states are represented with the appropriate momenta (spin indices omitted) as viewed from the barycentric system. In Eq. (2.2), E_i (E_f) is the initial (final) energy of the two-nucleon system. The energy of the two-nucleon system is initially the same as the energy in the barycentric system. In the final state the energy of the two-nucleon system is altered from that of the initial state by the photon energy. The nuclear Hamiltonian is represented by

$$H_N=K_1+K_2+V_N=H_0+V_N, \quad (2.3)$$

and the Lippman-Schwinger equations for the nuclear T matrix and the free-particle Green's function are given by

$$T_N(E)=V_N+V_NG_0(E)T_N(E) \quad (2.4)$$

and

$$G_0(E)=(E-H_0+i\eta)^{-1}. \quad (2.5)$$

Complete sets of intermediate plane-wave states are inserted in the first two terms of Eq. (2.2); it is not convenient to follow this procedure for the rescattering contribution, which is the third term of Eq. (2.2), since momentum conservation does not limit the number of intermediate states available, as is the case in the first two terms. The results are

$$\begin{aligned}T_{fi}=&\langle \mathbf{p}_{1f}\mathbf{p}_{2f} \mid V_{\rm em}G_0(E_i) \mid \mathbf{p}_{1f}+\mathbf{K}, \mathbf{p}_{2f}\rangle\langle \mathbf{p}_{1f}+\mathbf{K}, \mathbf{p}_{2f} \mid T_N(E_i) \mid \mathbf{p}_{1i}\mathbf{p}_{2i}\rangle\\ &+\langle \mathbf{p}_{1f}\mathbf{p}_{2f} \mid V_{\rm em}G_0(E_i) \mid \mathbf{p}_{1f}, \mathbf{p}_{2f}+\mathbf{K}\rangle\langle \mathbf{p}_{1f}, \mathbf{p}_{2f}+\mathbf{K} \mid T_N(E_i) \mid \mathbf{p}_{1i}\mathbf{p}_{2i}\rangle\\ &+\langle \mathbf{p}_{1f}\mathbf{p}_{2f} \mid T_N^{\ddagger}(E_f)G_0(E_f) \mid \mathbf{p}_{1i}-\mathbf{K}, \mathbf{p}_{2i}\rangle\langle \mathbf{p}_{1i}-\mathbf{K}, \mathbf{p}_{2i} \mid V_{\rm em} \mid \mathbf{p}_{1i}\mathbf{p}_{2i}\rangle\\ &+\langle \mathbf{p}_{1f}\mathbf{p}_{2f} \mid T_N^{\ddagger}(E_f)G_0(E_f) \mid \mathbf{p}_{1i}, \mathbf{p}_{2i}-\mathbf{K}\rangle\langle \mathbf{p}_{1i}, \mathbf{p}_{2i}-\mathbf{K} \mid V_{\rm em} \mid \mathbf{p}_{1i}\mathbf{p}_{2i}\rangle\\ &+\langle \mathbf{p}_{1f}\mathbf{p}_{2f} \mid T_N^{\ddagger}(E_f)G_0(E_f)V_{\rm em}G_0(E_i)T_N(E_i) \mid \mathbf{p}_{1i}\mathbf{p}_{2i}\rangle. \quad (2.6)\end{aligned}$$

The five T-matrix elements of Eq. (2.6) are represented by the five T-matrix diagrams of Fig. 1, respectively, if we define

$$T_{fi}=\langle \mathbf{p}_{1f}\mathbf{p}_{2f} \mid T^{(1)}+T^{(2)}+T^{(3)}+T^{(4)}+T^{(5)} \mid \mathbf{p}_{1i}\mathbf{p}_{2i}\rangle \quad (2.7)$$

in order of appearance in Eq. (2.6). Separation of the elements of the T matrix of Eq. (2.6) into relative and c.m. coordinates of the two-nucleon system is desirable because the nuclear matrix elements are defined with respect to the two-nucleon c.m. In diagrams 1 and 2 of Fig. 1, the photon is emitted after the nuclear interaction, and the two-nucleon c.m. system is identical to the barycentric system. In diagrams 3 and 4 of Fig. 1, the photon is emitted before the nuclear interaction, and the two-nucleon system has momentum relative to the barycentric system. The three reference frames involved in the calculation are then the laboratory frame, the barycentric system or the two-nucleon c.m. system before the photon is emitted, and the two-nucleon system after the photon is emitted. The transformation from the barycentric system to the laboratory frame is made relativistically, consistent with the relativistic treatment of the two-nucleon kinematics in on-the-energy-shell potential-model calculations. Strictly speaking, the transformation from the barycentric system to the final two-nucleon c.m. system should also be made relativistically. It is, however, a good approximation[29] to make this second transformation nonrelativistically, in which case the two-nucleon c.m. momentum is $-\mathbf{K}$, relative to the barycentric system. This is a result of the condition

$$\mathbf{p}_{1i}+\mathbf{p}_{2i}=\mathbf{p}_{1f}+\mathbf{p}_{2f}+\mathbf{K}=0, \quad (2.8)$$

which defines the barycentric frame. For the nonrelativistic transformation there is no singlet-triplet spin mixing as would occur for the relativistic transformation.

The use of a potential to represent the nuclear interaction makes this dynamical aspect of the present calculation unavoidably nonrelativistic. The nuclear matrix elements of $T^{(1)}$ and $T^{(2)}$ are calculated in the barycentric system, while the nuclear matrix elements of $T^{(3)}$ and $T^{(4)}$ are calculated in the final two-nucleon

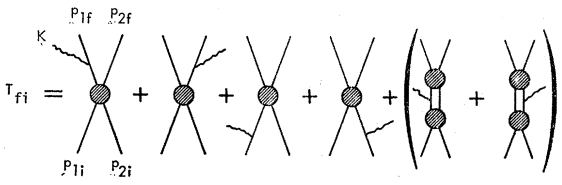

FIG. 1. The T-matrix diagrams for p-p-γ to first order in the electromagnetic interaction including rescattering. The labeling of the kinematics here corresponds to the barycentric system in the notation of Secs. II–V.

[28] The ‡ (double dagger) notation is a combination of two operations, complex conjugation and Hermitian conjugation, as introduced in Ref. 27.

[29] The maximum value of the relativistic velocity of the final p-p system with respect to the barycentric system at 160 MeV, for example, can be obtained by assuming that the photon takes all the kine ic energy, in which case $\beta<80/2m_p=0.05$.

c.m. system. The connection between these two systems by a nonrelativistic transformation allows a separation of the elements of the T matrix of Eq. (2.6), including $V_{\rm em}$, into relative and c.m. coordinates of the two-nucleon system. The integration over the coordinates of the c.m. motion with respect to the barycentric system exhibits the δ function for over-all conservation of momentum. In the notation of Eq. (2.7) the result is[30]

$$T_{fi}^{(1)}=\frac{\langle\phi_{\mathbf{k}_f}\mid V_{\rm em}\mid\phi_{-\mathbf{p}_{2f}}\rangle\langle\phi_{-\mathbf{p}_{2f}}\mid V_N\mid\psi_{\mathbf{k}_i}{}^{+}\rangle}{\tau(k_i)-\tau(p_{2f})},\tag{2.9}$$

$$T_{fi}^{(2)}=\frac{\langle\phi_{\mathbf{k}_f}\mid V_{\rm em}\mid\phi_{\mathbf{p}_{1f}}\rangle\langle\phi_{\mathbf{p}_{1f}}\mid V_N\mid\psi_{\mathbf{k}_i}{}^{+}\rangle}{\tau(k_i)-\tau(p_{1f})},\tag{2.10}$$

$$T_{fi}^{(3)}=\frac{\langle\psi_{\mathbf{k}_f}{}^{-}\mid V_N\mid\phi_{\mathbf{p}_{1i}-\mathbf{K}/2}\rangle\langle\phi_{\mathbf{p}_{1i}-\mathbf{K}/2}\mid V_{\rm em}\mid\phi_{\mathbf{k}_i}\rangle}{\tau(k_f)-\tau(p_{1i}-\frac{1}{2}K)},\tag{2.11}$$

$$T_{fi}^{(4)}=\frac{\langle\psi_{\mathbf{k}_f}{}^{-}\mid V_N\mid\phi_{\mathbf{p}_{1i}+\mathbf{K}/2}\rangle\langle\phi_{\mathbf{p}_{1i}+\mathbf{K}/2}\mid V_{\rm em}\mid\phi_{\mathbf{k}_i}\rangle}{\tau(k_f)-\tau(p_{1i}+\frac{1}{2}K)},\tag{2.12}$$

and

$$T_{fi}^{(5)}=\langle\psi_{\mathbf{k}_f}{}^{-}-\phi_{\mathbf{k}_f}\mid V_{\rm em}\mid\psi_{\mathbf{k}_i}{}^{+}-\phi_{\mathbf{k}_i}\rangle,\tag{2.13}$$

where $\psi_{\mathbf{k}_i}{}^{+}$ ($\psi_{\mathbf{k}_f}{}^{-}$) is the exact scattering state of the nucleon-nucleon system corresponding to outgoing (incoming) spherical wave boundary conditions, and $\phi_{\mathbf{q}}$ represents the various plane-wave states with the appropriate values of $\mathbf{q}$ indicated. All quantities in Eqs. (2.9)–(2.13), including $V_{\rm em}$ and the energy denominators, are now expressed in relative c.m. coordinates and momenta as determined from the barycentric system; correspondingly, we have introduced $\mathbf{k}_i=\mathbf{p}_{1i}$ and $\mathbf{k}_f=\frac{1}{2}(\mathbf{p}_{1f}-\mathbf{p}_{2f})$. In the above equations we have also introduced the quantity

$$\tau(k)=2m_p(\gamma_k-1),\tag{2.14}$$

where m_p is the mass of the proton and γ_k is the Lorentz contraction factor corresponding to a proton with momentum $\mathbf{k}$.

The electromagnetic potential $V_{\rm em}$ as used in Eqs. (2.9)–(2.13) is[31]

$$V_{\rm em}=e/m_p(2\pi/K)^{1/2}(e^{-i(\mathbf{K}\cdot\mathbf{r})/2}-e^{i(\mathbf{K}\cdot\mathbf{r})/2})i\boldsymbol{\varepsilon}\cdot\boldsymbol{\nabla}$$
$$+i\mu_p(2\pi/K)^{1/2}(e^{-i(\mathbf{K}\cdot\mathbf{r})/2}\boldsymbol{\sigma}_1\cdot\mathbf{K}\times\boldsymbol{\varepsilon}+e^{i(\mathbf{K}\cdot\mathbf{r})/2}\boldsymbol{\sigma}_2\cdot\mathbf{K}\times\boldsymbol{\varepsilon}),\tag{2.15}$$

where $e=(1/137.04)^{1/2}$ is the charge, $\mu_p=2.793e/2m_p$ is the magnetic moment of the proton, $\boldsymbol{\sigma}_1$ and $\boldsymbol{\sigma}_2$ are the Pauli spin operators of the protons, and $\boldsymbol{\varepsilon}$ is the polarization of the photon. Here we have chosen the Coulomb gauge so that $\mathbf{K}\cdot\boldsymbol{\varepsilon}=0$, and $V_{\rm em}$ as given in Eq. (2.15) is developed from the coupling of the electromagnetic field to the proton currents in the usual way,[32] using the principle of minimal electromagnetic coupling in the kinetic-energy part of the Hamiltonian only. For the Bryan-Scott potential this prescription is not gauge-invariant for the momentum-dependent part of the potential and will ultimately have to be suitably modified. In the following sections we shall refer to that part of the interaction (2.15) that corresponds to charge coupling of the protons to the electromagnetic field as the electric part $\mathcal{E}$, while the magnetic-moment coupling term shall be referred to as the magnetic term $\mathfrak{M}$, so that Eq. (2.15) can be written $V_{\rm em}=\mathcal{E}+\mathfrak{M}$.

III. SPIN AND POLARIZATION TREATMENT

In the barycentric system the z direction is taken as the photon direction, and the polarization states of the photon are represented in the circular basis corresponding to left and right circular polarization. The choice of the helicity representation for the photon is particularly convenient in the treatment of the rescattering term which is discussed in Sec. V. The singlet-triplet nuclear spin representation is used for the proton-proton system.

The electromagnetic matrix elements of Eqs. (2.9)–(2.12) correspond to that portion of the first four T-matrix diagrams where the photon is emitted from an external leg. The evaluation of the spatial part of these elements exhibits momentum conservation at each electromagnetic vertex, giving

$$\langle\mathbf{k}_fS_f\nu_f\mid T^{(1)}\mid\mathbf{k}_iS_i\nu_i\rangle=\frac{\langle\chi_{S_f\nu_f}\mid a_e\boldsymbol{\varepsilon}\cdot\mathbf{p}_{2f}+ia_m\boldsymbol{\sigma}_1\cdot\mathbf{K}\times\boldsymbol{\varepsilon}\mid\chi_{S'\nu'}\rangle\langle\phi_{-\mathbf{p}_{2f}S'\nu'}\mid V_N\mid\psi_{\mathbf{k}_iS_i\nu_i}{}^{+}\rangle}{\tau(k_i)-\tau(p_{2f})},\tag{3.1}$$

$$\langle\mathbf{k}_fS_f\nu_f\mid T^{(2)}\mid\mathbf{k}_iS_i\nu_i\rangle=\frac{\langle\chi_{S_f\nu_f}\mid a_e\boldsymbol{\varepsilon}\cdot\mathbf{p}_{1f}+ia_m\boldsymbol{\sigma}_2\cdot\mathbf{K}\times\boldsymbol{\varepsilon}\mid\chi_{S'\nu'}\rangle\langle\phi_{\mathbf{p}_{1f}S'\nu'}\mid V_N\mid\psi_{\mathbf{k}_iS_i\nu_i}{}^{+}\rangle}{\tau(k_i)-\tau(p_{1f})},\tag{3.2}$$

$$\langle\mathbf{k}_fS_f\nu_f\mid T^{(3)}\mid\mathbf{k}_iS_i\nu_i\rangle=\frac{\langle\psi_{\mathbf{k}_fS_f\nu_f}{}^{-}\mid V_N\mid\phi_{\mathbf{p}_{1i}-\mathbf{K}/2,S'\nu'}\rangle\langle\chi_{S'\nu'}\mid-a_e\boldsymbol{\varepsilon}\cdot\mathbf{k}_i+ia_m\boldsymbol{\sigma}_1\cdot\mathbf{K}\times\boldsymbol{\varepsilon}\mid\chi_{S_i\nu_i}\rangle}{\tau(k_f)-\tau(p_{1i}-\frac{1}{2}K)},\tag{3.3}$$

$$\langle\mathbf{k}_fS_f\nu_f\mid T^{(4)}\mid\mathbf{k}_iS_i\nu_i\rangle=\frac{\langle\psi_{\mathbf{k}_fS_f\nu_f}{}^{-}\mid V_N\mid\phi_{\mathbf{p}_{1i}+\mathbf{K}/2,S'\nu'}\rangle\langle\chi_{S'\nu'}\mid a_e\boldsymbol{\varepsilon}\cdot\mathbf{k}_i+ia_m\boldsymbol{\sigma}_2\cdot\mathbf{K}\times\boldsymbol{\varepsilon}\mid\chi_{S_i\nu_i}\rangle}{\tau(k_f)-\tau(p_{1i}+\frac{1}{2}K)},\tag{3.4}$$

[30] Further detail can be found in the University of California Radiation Laboratory Report No. UCRL-71263 (unpublished).
[31] Units of $\hbar=c=1$ are used throughout.
[32] R. P. Feynman, *Quantum Electrodynamics* (W. A. Benjamin, Inc., New York, 1961).

where spin indices are now included, and the two-nucleon spin state is given by $\chi_{S\nu}$, where S is the singlet or triplet spin and ν is the spin projection along the photon direction. The plane-wave normalization

$$\phi_{\mathbf{k}S\nu}=(2\pi)^{-3/2}e^{i\mathbf{k}\cdot\mathbf{r}}\chi_{S\nu} \tag{3.5}$$

is used in the evaluation of the electromagnetic integrals. In the above equations the quantities $a_e=e/m_p(2\pi/K)^{1/2}$ and $a_m=\mu_p(2\pi/K)^{1/2}$ are introduced.

Right- (left-) handed circular polarization for the photon is defined in the present convention by

$$\boldsymbol{\varepsilon}^{R(L)}=\tfrac{1}{2}\sqrt{2}(\boldsymbol{\varepsilon}_x\pm i\boldsymbol{\varepsilon}_y), \tag{3.6}$$

with the upper (lower) sign taken for right (left) handedness. The effect of using the helicity representation is to project out from the magnetic term $\mathfrak{M}$ of $V_{\rm em}$ either the raising or lowering spin operators for the nucleons. For example, the magnetic part of $V_{\rm em}$, appearing in Eqs. (3.1)–(3.4), for which we introduce the notation $\mathfrak{M}(\sigma)$ to indicate that the spatial integrals have been completed, becomes for right-handed circular polarization

$$\mathfrak{M}^R(\sigma)=ia_m\boldsymbol{\delta}_j\cdot\mathbf{K}\times\boldsymbol{\varepsilon}^R=a_mK\sigma_j{}^+, \tag{3.7}$$

where

$$\sigma_j{}^+=\tfrac{1}{2}\sqrt{2}(\sigma_{jx}+i\sigma_{jy})$$

is the usual Pauli-spin raising operator and j is the index designating the protons. The effect of $\sigma_j{}^+$ operating on the singlet and triplet states is given by

$$\sigma_j{}^+\chi_{00}=(-1)^j\chi_{11},\qquad \sigma_j{}^+\chi_{11}=0,$$

and

$$\sigma_j{}^+\chi_{1\nu}=\delta_{\nu 0}\chi_{11}+\delta_{\nu,-1}[\chi_{10}+(-1)^{j+1}\chi_{00}]. \tag{3.8}$$

The fact that the electromagnetic interaction mixes the singlet-triplet spin states can be seen from Eq. (3.8); however, transitions between the singlet and triplet spin states do not occur for the nuclear matrix elements. Certain selection rules are evident in considering over-all transitions of the two-nucleon system from the initial to the final state as in Eqs. (3.1)–(3.4). Over-all singlet-singlet transitions are purely electric, while over-all singlet-triplet transitions are purely magnetic. For over-all triplet-singlet transitions in which the two nucleons are initially in the triplet state, the nuclear matrix elements of Eqs. (3.1) and (3.2), which represent the case in which the photon is emitted after the nuclear interaction, involve triplet states only. On the other hand, when the photon is emitted before the nuclear interaction as in Eqs. (3.3) and (3.4), the nuclear matrix elements involve only singlet states. The reverse of this is true in over-all singlet-triplet transitions in which the two nucleons are initially in the singlet state; that is, the nuclear matrix elements of Eqs. (3.1) and (3.2) involve only singlet states, and those of Eqs. (3.3) and (3.4) involve only triplet states. For over-all triplet transitions of the two-nucleon system, there are both electric and magnetic contributions, and the nuclear matrix elements involve triplet states only. The left-handed circular polarization involves lowering operators and corresponding spin transition selection rules.

IV. NUCLEAR MATRIX ELEMENTS

The off-energy-shell nuclear matrix elements which are needed in Eqs. (3.1)–(3.4) can be calculated in terms of surface and volume contributions, eliminating the necessity of integrating over the nuclear potential. Consider a nuclear matrix element of the form in Eqs. (3.1) and (3.2) (omitting spin indices):

$$T_N=(\phi_{\mathbf{q}},\, V_N\psi_{\mathbf{k}}{}^+). \tag{4.1}$$

Because of the finite extent of the nuclear interaction the integral over all space of Eq. (4.1) can be replaced with

$$T_N=\int_0^R\phi_{\mathbf{q}}{}^*V_N\psi_{\mathbf{k}}{}^+d\mathbf{r}, \tag{4.2}$$

where R is beyond the range of the nuclear interaction. Adding and subtracting ∇^2/m_p to V_N and using

$$(-\nabla^2/m_p+V_N)\psi_{\mathbf{k}}{}^+=E_k\psi_{\mathbf{k}}{}^+$$

yields

$$T_N=\int_0^R\phi_{\mathbf{q}}{}^*E_k(\psi_{\mathbf{k}}{}^+-\phi_{\mathbf{k}})\,d\mathbf{r}+\int_0^R\phi_{\mathbf{q}}{}^*\nabla^2/m_p(\psi_{\mathbf{k}}{}^+-\phi_{\mathbf{k}})d\mathbf{r}, \tag{4.3}$$

where the plane wave has been subtracted for convenience. The second term in Eq. (4.3) can be further reduced to a volume and surface contribution, resulting in

$$T_N=(E_k-E_q)\int_0^R\phi_{\mathbf{q}}{}^*(\psi_{\mathbf{k}}{}^+-\phi_{\mathbf{k}})\,d\mathbf{r}$$
$$+m_p{}^{-1}\int_S d\Omega\,R^2\left(\phi_{\mathbf{q}}{}^*\frac{\partial}{\partial r}(\psi_{\mathbf{k}}{}^+-\phi_{\mathbf{k}})-\frac{\partial\phi_{\mathbf{q}}{}^*}{\partial r}(\psi_{\mathbf{k}}{}^+-\phi_{\mathbf{k}})\right)_{r=R}. \tag{4.4}$$

The volume term of Eq. (4.4) goes to zero on the energy shell or in the limit of no photon emission. The surface term, which is evaluated beyond the range of the nuclear interaction, is directly expressible in terms of phase shifts and scattering parameters for the partial waves corresponding to the two-nucleon c.m. momentum $\mathbf{k}$. The treatment of the nuclear matrix elements of Eqs. (3.3) and (3.4) involving $\psi_{\mathbf{k}_f}{}^-$ follows in a similar fashion.

Because of the tensor force the nuclear Hamiltonian does not commute with $\mathbf{L}^2$, but it does commute with

$\mathbf{S}^2$, $\mathbf{J}^2$, J_z, and the parity operator. Accordingly, the nuclear scattering states can be resolved into states of well-defined total angular momentum, its projection along the axis of quantization, well-defined total spin, and parity. The partial-wave decomposition of the nuclear scattering states with incoming (outgoing) spherical wave boundary conditions for c.m. momentum $\mathbf{k}$ and total spin S with component ν along the axis of quantization, which is taken as the photon direction, is then

$$\psi_{\mathbf{k}S\nu}{}^{+(-)}=\sum_{JMl'l} C_{m\nu M}{}^{lSJ} y_l{}^{m*}(\hat{k})\mathcal{Y}_{Jl'S}{}^{M}(\hat{r})\psi_{l'l;JS}{}^{+(-)}(kr), \tag{4.5}$$

where we have introduced the well-known vector-addition coefficients,[33] the spherical harmonics,[34] and the spin-angle functions[35] which are simultaneous eigenfunctions of $\mathbf{J}^2$ and J_z, defined by

$$\mathcal{Y}_{Jl'S}{}^{M}(\hat{r})=\sum_{\nu'm'} C_{m'\nu'M}{}^{l'SJ} y_{l'}{}^{m'}(\hat{r})\chi_{S\nu'}. \tag{4.6}$$

Because of tensor coupling of orbital angular momentum the radial wave function of Eq. (4.5) is designated by both l and l', where l' would be the angular momentum in the absence of the tensor force. The identity of the protons requires totally antisymmetric states restricting orbital angular momentum to even (odd) values in singlet (triplet) states. The analogous decomposition into partial waves of a plane-wave state with c.m. momentum $\mathbf{q}$ and total spin S with component ν along the axis of quantization can be written

$$\phi_{\mathbf{q}S\nu}=\sum_{lJM} C_{m\nu M}{}^{lSJ} y_l{}^{m*}(\hat{q})\mathcal{Y}_{Jls}{}^{M}(\hat{r})\phi_l(qr), \tag{4.7}$$

where we have introduced

$$\phi_l(qr)=(2/\pi)^{1/2} i^l j_l(qr). \tag{4.8}$$

The evaluation of the nuclear matrix elements of Eqs. (3.1)–(3.4) can be made in terms of surface and volume contributions with the use of Eqs. (4.4)–(4.8). Spin indices are now included for a general case; total spin is not mixed by the nuclear interaction, but when $S=1$, the spin projection ν is mixed by the tensor force. The results corresponding to the nuclear matrix elements of Eqs. (3.1) and (3.2) are

$$\langle \mathbf{q}S\nu' \mid T_N \mid \mathbf{k}S\nu\rangle = \sum_{JMl'l} C_{m'\nu'M}{}^{l'SJ} C_{m\nu M}{}^{lSJ} y_{l'}{}^{m'}(\hat{q})\, y_l{}^{m*}(\hat{k})\,(\mathcal{U}+\mathcal{S}), \tag{4.9}$$

where

$$\mathcal{U}=(E_k-E_q)\int_0^R \phi_{l'}{}^{*}(qr)[\psi_{l'l;JS}{}^{+}(kr)-\delta_{l'l}\phi_{l'}(kr)]r^2dr \tag{4.10}$$

and

$$\mathcal{S}=\frac{R^2}{m_p}\left(\phi_{l'}{}^{*}(qr)\frac{\partial}{\partial r}[\psi_{l'l;JS}{}^{+}(kr)-\delta_{l'l}\phi_{l'}(kr)] - \frac{\partial}{\partial r}\phi_{l'}{}^{*}(qr)[\psi_{l'l;JS}{}^{+}(kr)-\delta_{l'l}\phi_{l'}(kr)]\right)_{r=R}. \tag{4.11}$$

In obtaining the results in Eq. (4.9) we have made use of the orthogonality of the spin-angle functions given by

$$\int [\mathcal{Y}_{Jls}{}^{M}(\hat{r})]^{\dagger}\mathcal{Y}_{J'l'S}{}^{M'}(\hat{r})\,d\Omega=\delta_{J'J}\delta_{M'M}\delta_{l'l}. \tag{4.12}$$

The results for the evaluation of the nuclear matrix elements of Eqs. (3.3) and (3.4) are similar to those given by Eq. (4.9), where use is made of the energy-shell relationship[36]

$$\psi_{l'l;JS}{}^{-}(kr)=(-1)^{l'}[\psi_{l'l;JS}{}^{+}(kr)]^{*}, \tag{4.13}$$

which can be obtained by time-reversal considerations.

The evaluation of the radial portions of the nuclear matrix elements as given by the volume and surface contributions of Eqs. (4.10) and (4.11) does not explicitly involve the nuclear potential. The determination of the volume contribution requires a numerical integration, involving the two-nucleon wave functions, out to some point R beyond the range of the nuclear interaction. The surface contribution of the radial integrals is evaluated beyond the range of the nuclear interaction, allowing the replacement of the two-nucleon scattering states by their asymptotic forms, where, in the present study, the Blatt-Biedenharn parametrization[37] is used. On the energy shell ($k=q$) the radial portions of the nuclear matrix elements which are obtained from the surface integrals of Eq. (4.11) reduce to the same expressions as given for the on-energy-shell matrix elements by Stapp *et al.*[38] It is also useful to point out that the quasiphase parameters introduced by Cromer and Sobel[14] take a particularly convenient form when expressed in terms of volume and surface integrals in the manner developed above, where again the necessity of integrating over the nuclear potential is eliminated.

V. RESCATTERING

The fifth diagram of Fig. 1 (in parentheses) is the rescattering term and is expressed by Eq. (2.13).

[33] A. R. Edmonds, *Angular Momentum in Quantum Mechanics* (Princeton University Press, Princeton, N.J., 1957).
[34] The phase convention $y_l{}^{m*}=(-1)^m y_l{}^{-m}$ is used here.
[35] J. M. Blatt and V. F. Weisskopf, *Theoretical Nuclear Physics* (John Wiley & Sons, Inc., New York, 1958).
[36] M. L. Goldberg and K. M. Watson, *Collision Theory* (John Wiley & Sons, Inc., New York, 1964).
[37] J. M. Blatt and L. C. Biedenharn, Rev. Mod. Phys. **24**, 258 (1952).
[38] H. P. Stapp, T. J. Ypsilantis, and N. Metropolis, Phys. Rev. **105**, 302 (1957).

Whereas $V_{\rm em}$ was evaluated between plane-wave states, giving δ-function momentum conservation for the first four diagrams of Fig. 1, for the fifth diagram $V_{\rm em}$ is evaluated between the distorted parts of the nuclear scattering states, that is, with the undistorted momentum eigenstates subtracted out, portending a solution by partial-wave analysis. The feasibility of this approach stems from the fact that the plane waves subtracted from the initial and final states provide cutoffs in the respective partial-wave decompositions of these states, thereby providing a cutoff in the partial-wave decomposition of $V_{\rm em}$.

The electric part $\mathcal{E}$ of the electromagnetic potential of Eq. (2.15) for right-handed circular polarization of the photon is given by

$$\mathcal{E}^R=a_e(e^{-i(\mathbf{K}\cdot\mathbf{r})/2}-e^{i(\mathbf{K}\cdot\mathbf{r})/2})i\boldsymbol{\varepsilon}^R\cdot\boldsymbol{\nabla}, \tag{5.1}$$

where for use in spherical polar coordinates we can write

$$\boldsymbol{\varepsilon}^R\cdot\boldsymbol{\nabla}=-(\tfrac{4}{3}\pi)^{1/2}y_1{}^1(\hat{r})\left(\frac{\partial}{\partial r}-\frac{L_z}{r}\right)+(\tfrac{2}{3}\pi)^{1/2}y_1{}^0(\hat{r})\frac{L^+}{r}. \tag{5.2}$$

In Eq. (5.2) the usual orbital angular momentum operators L^+ and L_z are introduced, where

$$L^+y_l{}^m(\hat{r})=[(l-m)(l+m+1)]^{1/2}y_l{}^{m+1}(\hat{r}) \tag{5.3}$$

and

$$L_zy_l{}^m(\hat{r})=my_l{}^m(\hat{r}). \tag{5.4}$$

The results of $\mathcal{E}^R$ operating on the product of a radial function and a spherical harmonic, as in the case of a two-nucleon scattering state, can be written

$$\begin{aligned}\mathcal{E}^Rf_l(r)y_l{}^m(\hat{r})=&\sqrt{2}a_e\sin(\mathbf{K}\cdot\mathbf{r}/2)\\&\times\left\{-\left[\frac{(l+m+1)(l+m+2)}{(2l+3)(2l+1)}\right]^{1/2}y_{l+1}{}^{m+1}(\hat{r})\right.\\&\times\left(\frac{\partial f_l(r)}{\partial r}-l\frac{f_l(r)}{r}\right)+\left[\frac{(l-m-1)(l-m)}{(2l+1)(2l-1)}\right]^{1/2}\\&\left.\times y_{l-1}{}^{m+1}(\hat{r})\left(\frac{\partial f_l(r)}{\partial r}+(l+1)\frac{f_l(r)}{r}\right)\right\}.\end{aligned} \tag{5.5}$$

It is useful to note that when $f_l(r)$ is a Bessel function, the expressions in parentheses on the right-hand side of Eq. (5.5) can be simplified by recursion relations.

The magnetic part $\mathfrak{M}$ of $V_{\rm em}$ of Eq. (2.15) for right-handed circular polarization of the photon is given by

$$\mathfrak{M}^R=a_mK(e^{-i(\mathbf{K}\cdot\mathbf{r})/2}\sigma_1{}^++e^{i(\mathbf{K}\cdot\mathbf{r})/2}\sigma_2{}^+). \tag{5.6}$$

The results of $\mathfrak{M}^R$ operating on the singlet-triplet spin states and expanded in partial waves are given by

$$\mathfrak{M}^R\chi_{00}=a_mK\left(2\sum_l{}^{\rm odd}i^l[4\pi(2l+1)]^{1/2}j_l(\tfrac{1}{2}Kr)y_l{}^0(\hat{r})\right)\chi_{11}, \tag{5.7}$$

$$\mathfrak{M}^R\chi_{11}=0, \tag{5.8}$$

$$\mathfrak{M}^R\chi_{10}=a_mK\left(2\sum_l{}^{\rm even}i^l[4\pi(2l+1)]^{1/2}j_l(\tfrac{1}{2}Kr)y_l{}^0(\hat{r})\right)\chi_{11}, \tag{5.9}$$

and

$$\begin{aligned}\mathfrak{M}^R\chi_{1,-1}=&a_mK\left(2\sum_l{}^{\rm even}i^l[4\pi(2l+1)]^{1/2}j_l(\tfrac{1}{2}Kr)y_l{}^0(\hat{r})\right)\chi_{10}\\&+a_mK\left(2\sum_l{}^{\rm odd}i^l[4\pi(2l+1)]^{1/2}j_l(\tfrac{1}{2}Kr)y_l{}^0(\hat{r})\right)\chi_{00}.\end{aligned} \tag{5.10}$$

In the evaluation of the nuclear matrix elements discussed in Sec. IV, the orthogonality of the spin-angle functions considerably simplified the resulting expressions. In the rescattering term the angular integrations involve the spherical harmonics of $V_{\rm em}$ as well as those in the nuclear states, and $\mathcal{E}^R$ contains orbital angular momentum operators which act on the spherical harmonics in the expansion of the spin-angle functions of Eq. (4.5). Consequently, to calculate rescattering, the nuclear wave functions are expressed as in Eq. (4.5), but including the expanded form of the spin-angle functions as given in Eq. (4.6).

The rescattering contribution for the electric part $\mathcal{E}^R$ of $V_{\rm em}$ (following angular integrations) is given by

$$\begin{aligned}&\langle\psi_{\mathbf{k}_f S_f\nu_f}{}^--\phi_{\mathbf{k}_f S_f\nu_f}\,|\,\mathcal{E}^R\,|\,\psi_{\mathbf{k}_i S_i\nu_i}{}^+-\phi_{\mathbf{k}_i S_i\nu_i}\rangle\\&=-i\sqrt{2}a_e\delta_{S_iS_f}\sum_{l_e}{}^{\rm odd}\sum_{J_fl_f'l_f,M_f\nu_f'}\sum_{J_il_i'l_i,M_i\nu_i'}\delta_{\nu_i'\nu_f'}(2l_i'+1)^{-1}\\&\times\mathcal{C}^{l_e}(m_j(l_j,S_j)J_j;\hat{k}_i,\hat{k}_f)\sum_{\lambda=l_i'\pm1}\{\mp[\lambda\pm(m-1)]^{1/2}\\&\times[(\lambda+1)\pm(m-1)]^{1/2}C_{m0m_f,}{}^{\lambda l_el_f'}C_{000}{}^{\lambda l_el_f'}\\&\times[\mathcal{R}_1+((1-\lambda)\delta_{\lambda,l_i'+1}+(2+\lambda)\delta_{\lambda,l_i'-1})\mathcal{R}_2]\},\end{aligned} \tag{5.11}$$

where λ takes on the values $l_i'\pm1$ with the upper (lower) sign corresponding to $l_i'+1$ ($l_i'-1$) throughout, and $m=m_i'+1$. The sums over magnetic quantum numbers M_f, M_i, ν_f', and ν_i' have the restrictions

$$M_i=m_i'+\nu_i'=m_i+\nu_i \tag{5.12}$$

and

$$M_f=m_f'+\nu_f'=m_f+\nu_f. \tag{5.13}$$

In Eq. (5.11) we have introduced

$$\mathfrak{A}^{l_e}(m_j(l_jS_j)J_j;\hat{k}_i\hat{k}_f)=i^{l_e}(2l_e+1)[(2l_i'+1)/(2l_f'+1)]^{1/2}$$
$$\times y_{l_f}^{m_f}(\hat{k}_f)\,y_{l_i}^{m_i*}(\hat{k}_i)\,C_{m_f\nu_fM_f}^{\ \ l_fS_fJ_f}$$
$$\times C_{m_i\nu_iM_i}^{\ \ l_iS_iJ_i}C_{m_f'\nu_f'M_f}^{\ \ l_f'S_fJ_f}C_{m_i'\nu_i'M_i}^{\ \ l_i'S_iJ_i}, \quad (5.14)$$

where the dependence of $\mathfrak{A}$ on the various nuclear quantum numbers is indicated by the subscript j. The radial integrals $\mathfrak{R}_1$ and $\mathfrak{R}_2$ are given by

$$\mathfrak{R}_1=\int_0^\infty [\psi_{l_f'l_f;J_fS_f}^{-}(k_fr)-\delta_{l_fl_f'}\phi_{l_f'}(k_fr)]^*j_{l_e}(\tfrac{1}{2}Kr)$$
$$\times\frac{\partial}{\partial r}[\psi_{l_i'l_i;J_iS_i}^{+}(k_ir)-\delta_{l_i'l_i}\phi_{l_i'}(k_ir)]r^2dr \quad (5.15)$$

and

$$\mathfrak{R}_2=\int_0^\infty [\psi_{l_f'l_f;J_fS_f}^{-}(k_fr)-\delta_{l_f'l_f}\phi_{l_f'}(k_fr)]^*j_{l_e}(\tfrac{1}{2}Kr)$$
$$\times r^{-1}[\psi_{l_i'l_i;J_iS_i}^{+}(k_ir)-\delta_{l_i'l_i}\phi_{l_i'}(k_ir)]r^2dr. \quad (5.16)$$

The angular integration leading to Eq. (5.11) was performed with the use of

$$\int y_{l_f'}^{m_f'*}(\hat{r})\,y_{l_e}^{0}(\hat{r})\,y_\lambda^{m}(\hat{r})\,d\Omega$$
$$=\left(\frac{(2l_e+1)(2\lambda+1)}{4\pi(2l_f'+1)}\right)^{1/2}C_{m0m_f'}^{\ \ \lambda l_el_f'}C_{000}^{\ \ \lambda l_el_f'}, \quad (5.17)$$

where, in application to Eq. (5.11), $\lambda=l_i'\pm1$ and $m=m_i'+1$.

The indices of Eqs. (5.11)–(5.16) are subscripted by i and f to indicate the initial and final states; the quantum numbers which appear both primed and unprimed correspond to mixing by the nuclear interaction as discussed in Sec. IV. The sums over the various quantum numbers for the initial and final states have the restrictions described in Sec. IV in consideration of the identity of the p-p system. The sum over odd values of the index l_e represents the electromagnetic partial-wave decomposition of $\sin(\mathbf{K}\cdot\mathbf{r}/2)$ appearing in $\mathcal{E}^R$ of Eq. (5.5), corresponding again to taking the z axis along the photon direction $\mathbf{K}$. The cutoff in the partial-wave decomposition of the electromagnetic potential is determined by the number of partial waves needed to describe the distorted parts of the initial and final p-p scattering states. The vector-coupling coefficients in Eq. (5.11), which resulted from the angular integration according to Eq. (5.17), contain the specific rules for coupling $l_i'\pm1$, l_e, and l_f'.

Since $\mathcal{E}^R$ does not mix spin or spin projection, the orthogonality of the singlet-triplet spin eigenfunctions has been invoked, as evidenced by the Kronecker δ symbols involving spin indices, which appear in Eq. (5.11); the latter symbol restricts the sums on ν_i' and ν_f' to a single sum. Note that Eq. (5.11) is written for a particular spin transition so that S_i, S_f, ν_i, and ν_f are not summed over; consequently, the Kronecker δ symbol involving S_i and S_f on the right-hand side of the equation is interpreted according to the general nature of Eq. (5.11) in representing either singlet-singlet or triplet-triplet transitions. Now, since $M_i=m_i'+\nu_i'$ and $M_f=m_f'+\nu_f'$, the restriction $m_f'=m_i'+1$ exhibited by the angular integration combined with the fact that $\nu_i'=\nu_f'$ yields the result

$$M_f=M_i+1. \quad (5.18)$$

All the sums over magnetic quantum numbers that appear in Eq. (5.11) reduce then to a single sum involving only one magnetic quantum number.

The contribution to the rescattering term from the magnetic part of the electromagnetic interaction $\mathfrak{M}^R$ mixes the two-nucleon spin representation according to Eqs. (5.7)–(5.10). The matrix elements of $\mathfrak{M}^R$ involving singlet-singlet transitions of the two-nucleon system are forbidden, while transitions that connect the singlet and triplet states are allowed. In other words, as in the case of the selection rules corresponding to the first four T-matrix diagrams, singlet-singlet transitions are purely electric, and singlet-triplet transitions are purely magnetic. The rescattering matrix elements of $\mathfrak{M}^R$ for a given spin transition which involves transitions between the two-nucleon singlet and triplet spin states can be summarized by

$$\langle\psi_{\mathbf{k}_f S_f\nu_f}^{-}-\phi_{\mathbf{k}_f S_f\nu_f}\,|\,\mathfrak{M}^R\,|\,\psi_{\mathbf{k}_i S_i\nu_i}^{+}-\phi_{\mathbf{k}_i S_i\nu_i}\rangle=2a_mK\sum_{l_e}^{\text{odd}}\sum_{J_fl_f'l_f',M_f\nu_f'}\sum_{J_il_i'l_i,M_i\nu_i'}(\delta_{S_f1}\delta_{S_i0}\delta_{\nu_f'1}\delta_{\nu_i'0}+\delta_{S_f0}\delta_{S_i1}\delta_{\nu_f'0}\delta_{\nu_i'-1})$$
$$\times\mathfrak{A}^{l_e}(m_j(l_jS_j)J_j;\hat{k}_i,\hat{k}_f)C_{m_i'0m_f'}^{\ \ \ l_i'l_el_f'}C_{000}^{\ \ l_i'l_el_f'}\mathfrak{R}_3 \quad (5.19)$$

and

$$\mathfrak{R}_3=\int_0^\infty[\psi_{l_f'l_f;J_fS_f}^{-}(k_fr)-\delta_{l_f'l_f}\phi_{l_f'}(k_fr)]^*j_{l_e}(\tfrac{1}{2}Kr)[\psi_{l_i'l_i;J_iS_i}^{+}(k_ir)-\delta_{l_i'l_i}\phi_{l_i'}(k_ir)]r^2dr. \quad (5.20)$$

The results of the application of Eqs. (5.7) and (5.10) along with the orthogonality of the spin eigenfunctions in the development of Eq. (5.19) are summarized by the Kronecker δ symbols in the parentheses. For a particular singlet-triplet transition S_i, S_f, ν_i, and ν_f are given, and are therefore not summed over. In the present case Eq. (5.19) represents a general singlet-triplet spin transition where either the initial or the final state is the singlet; the Kronecker δ symbols involving S_i and S_f are included on the right-hand side of the equation to distinguish the two distinct cases. The first (second) term in the parentheses corresponds to the initial (final) state being the singlet; correspondingly, the sum on ν_i' (ν_f') is degenerate. Since either the initial or the final state is a singlet, the corresponding vector-coupling coefficients collapse to unity, and the quantum numbers necessary to describe the state are reduced to $J=l'=l$ and $M=m'=m$.

The angular integrations leading to Eq. (5.19) have been done according to Eq. (5.17), where now $\lambda=l_i'$ and $m=m_i'$. Accordingly, the vector-coupling coefficient from the angular integrations contain the coupling between l_i', l_e, and l_f', which limits the sum on l_e as in the case of the rescattering contribution involving $\mathcal{E}^R$. Also exhibited by the angular integrations is the restriction $m_i'=m_f'$. A consideration of the magnetic quantum numbers for the spin transitions represented by Eq. (5.19) leads to the result $M_f=M_i+1$ as given in Eq. (5.18), and appropriately the sum over magnetic quantum numbers reduces to a single sum.

The rescattering matrix elements of $\mathfrak{M}^R$ for triplet-triplet transitions can be written

$$\langle\psi_{\mathbf{k}_f S_f \nu_f}{}^- - \phi_{\mathbf{k}_f S_f \nu_f} \mid \mathfrak{M}^R \mid \psi_{\mathbf{k}_i S_i \nu_i}{}^+ - \phi_{\mathbf{k}_i S_i \nu_i}\rangle = 2a_m K \delta_{S_i 1}\delta_{S_f 1} \sum_{l_e}^{\text{even}} \sum_{J_f l_f' l_f, M_f \nu_f'} \sum_{J_i l_i' l_i, M_i \nu_i'} (\delta_{\nu_f' 0}\delta_{\nu_i',-1} + \delta_{\nu_f' 1}\delta_{\nu_i' 0})$$

$$\times \alpha^{l_e}(m_j(l_j S_j)J_j; \hat{k}_i\hat{k}_f) C_{m_i' 0 m_f', l_i' l_e l_f'} C_{000}{}^{l_i' l_e l_f'} \mathcal{R}_3. \quad (5.21)$$

The orthogonality of the spin eigenfunctions along with the results of Eqs. (5.8)–(5.10) have been used to obtain the Kronecker δ symbols of Eq. (5.21). For a given triplet-triplet transition ν_i and ν_f are fixed, and although $S_i=S_f=1$ throughout, the Kronecker δ symbols involving S_i and S_f are included on the right-hand side of Eq. (5.21) to be consistent with the earlier notation. The angular-integration results leading to the rescattering matrix elements of $\mathfrak{M}^R$ for triplet-triplet transitions are the same as those obtained for the singlet-triplet $\mathfrak{M}^R$ matrix elements of Eq. (5.19), where now l_e is summed over even values. The cutoff in l_e follows in the same fashion as described previously. For a given spin transition there are two separate contributions to Eq. (5.21) as evidenced by the two terms in parentheses involving ν_i' and ν_f'. A consideration of the magnetic quantum numbers for both contributions leads to the result $M_f=M_i+1$ as given in Eq. (5.18), and appropriately the sum over magnetic quantum numbers reduces again to a single sum.

The determination of the electric and magnetic rescattering contributions of Eqs. (5.11), (5.19), and (5.21) requires the integration over all space of the electromagnetic potential evaluated between the distorted parts of the initial and final exact scattering states of the two-nucleon system. The angular integrals exhibit the cutoff in the partial-wave decompositions described above. The three distinct types of radial integrals, all with limits from zero to infinity, are given by $\mathcal{R}_1$, $\mathcal{R}_2$, and $\mathcal{R}_3$ of Eqs. (5.15), (5.16), and (5.20). The radial parts of the $\mathcal{E}^R$ matrix elements given by $\mathcal{R}_1$ and $\mathcal{R}_2$ involve the spherical Bessel functions obtained from the partial-wave decomposition of the electromagnetic potential, along with the distorted parts of the initial and final radial wave functions. The $\mathcal{R}_1$ integrals contain a radial derivative of the initial state, whereas a weighting factor of r^{-1} is contained in the $\mathcal{R}_2$ integrals. The radial integrals $\mathcal{R}_3$ corresponding to the matrix elements of $\mathfrak{M}^R$ involve the distorted parts of the initial and final radial wave functions and the spherical Bessel functions of the electromagnetic potential, with no additional radial dependence. Inside the range of the nuclear interaction a numerical integration involving the appropriate nuclear wave functions and derivatives is performed. Beyond the range of the nuclear interaction the wave functions take on their asymptotic forms, and the problem reduces to the evaluation of integrals involving combinations of the product of three spherical Bessel and Neumann functions, with limits from a point beyond the range of the nuclear interaction to infinity. A typical integral is of the form

$$\int_R^\infty f_{l_f}(k_f r) j_{l_e}(\tfrac{1}{2}Kr) f_{l_i}(k_i r) r^2 dr, \quad (5.22)$$

where the initial and final functions designated by f can be either spherical Bessel or Neumann functions and R is a point beyond the range of the nuclear interaction. A method of evaluating these integrals in terms of sine and cosine integrals has been developed, the details of which are discussed elsewhere.[30]

The rescattering matrix elements as presented

throughout this section are expressed for a particular helicity state of the photon, corresponding to right-handed circular polarization. The effect of using the helicity state corresponding to the left-handed circular polarization of the photon is to project out lowering operators corresponding to the orbital angular momentum operator of $\mathcal{E}$ and the spin operators of $\mathfrak{M}$. The results for the left-handed helicity state follow in a similar fashion to those developed above, where, for example, the magnetic quantum number restriction of Eq. (5.18) becomes $M_f=M_i-1$.

The rescattering matrix elements expressed in this section can be evaluated utilizing irreducible tensor operators for the electromagnetic potential. The reduced matrix elements can be obtained using the Wigner-Eckart theorem eliminating some of the vector-coupling coefficients appearing in our formulas. These results are presented elsewhere.[30]

VI. CROSS SECTION

In Secs. II–V the T matrix for the p-p-γ process has been formulated entirely in the barycentric system. To compare to experimental results, which for the most part are coplanar in the laboratory, Moller's invariant form[36] of the cross section is introduced. Since for the p-p-γ experiments of present interest the incident beam and target are unpolarized and the final-state spins and polarizations are unobserved, the cross section contains an average over initial spins as well as a sum over final spins and polarizations, and is given by

$$d\sigma=\{\tfrac{1}{4}\sum_{\mu}\sum_{S_i\nu_i S_f\nu_f} 4\,|\,\langle S_f\nu_f\,|\,T_\mu\,|\,S_i\nu_i\rangle\,|^2 E_{1f}'E_{2f}'K'E_{1i}'E_{2i}'\}/\{E_{1i}E_{2i}\,|\,\beta_{1i}-\beta_{2i}\,|\,\}$$
$$\times\left\{(2\pi)^4\delta^3(\mathbf{p}_{1i}+\mathbf{p}_{2i}-\mathbf{p}_{1f}-\mathbf{p}_{2f}-\mathbf{K})\,\delta(E_{1i}+E_{2i}-E_{1f}-E_{2f}-K)\,\frac{d^3p_{1f}}{E_{1f}}\frac{d^3p_{2f}}{E_{2f}}\frac{d^3K}{(2\pi)^3K}\right\},\quad(6.1)$$

where the subscripted quantities correspond to the initial and final momenta, total energies, and spins of the two protons, and the energy and momentum of the emitted photon is given by K. The factor of 4 in Eq. (6.1) arises because of the antisymmetrization of the nuclear wave functions in Sec. IV corresponding to the identity of the two protons. The sum over the photon polarization extends over the two values of μ, and the normalization in the phase-space factor corresponds to that introduced earlier. The relativistic energy E and the momentum $\mathbf{p}$ for a given proton state as used in Eq. (6.1) are given by

$$E=p^2+m^2=m\gamma \quad\text{and}\quad \mathbf{p}=m\beta\gamma.\qquad(6.2)$$

Each term enclosed in curly brackets is an invariant; the numerator containing the T matrix is calculated in the barycentric system where the energies have been primed to distinguish them from laboratory quantities, and the remaining two invariants are calculated in the laboratory system.

The usual experimental situation is the coplanar symmetric geometry introduced by Gottschalk *et al.*,[3] referred to as the Harvard geometry, in which the final protons are observed in coincidence, at equal angles to, and in the same plane as, the incident beam, thereby restricting the photon to this plane as well. The diagram for the kinematics in the laboratory, which is now the unprimed system, is shown in Fig. 2.

Of special interest is the differential cross section $d\sigma/d\Omega_1 d\Omega_2 d\theta_\gamma$ corresponding to the photon angular distribution for fixed proton coplanar angles in the Harvard geometry. The determination of this cross section from the invariant form given in Eq. (6.1) can be obtained by first integrating over the photon azimuthal angle ϕ_γ and then over p_{1f} and p_{2f}, using the momentum δ function, followed by the integration over K, using the energy δ function, resulting in

$$\frac{d\sigma}{d\Omega_1 d\Omega_2 d\theta_\gamma}=\{\sum_{\mu}\sum_{S_i\nu_i S_f\nu_f}|\,\langle S_f\nu_f\,|\,T_\mu\,|\,S_i\nu_i\rangle\,|^2 E_{1f}'E_{2f}'K'E_{1i}'E_{2i}'\}/E_{1i}E_{2i}\,|\,\beta_{1i}-\beta_{2i}\,|$$
$$\times\left\{2\,\frac{(2\pi)\,p_{1f}\beta_{1f}p_{2f}\beta_{2f}K}{|\,\sin(\theta_1+\theta_2)+\beta_{2f}\sin(\theta_\gamma-\theta_1)-\beta_{1f}\sin(\theta_\gamma+\theta_2)\,|}\right\},\quad(6.3)$$

where a factor of 2 is introduced to allow for the two symmetric solutions corresponding to the photon being emitted up or down with respect to the beam.

A calculational simplification exists in the evaluation of the cross section for the present case, in which there is no initial polarization or observation of final spins. Invariance requirements including conservation of angular momentum, reflection symmetry, and the identity of the two protons, coupled with the coplanarity of the three-body final state of p-p-γ in the bary-

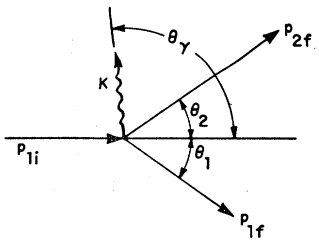

FIG. 2. Kinematics of p-p-γ in the Harvard geometry. Here p_{1i} is the incident proton momentum in the laboratory, p_{1f} and p_{2f} are the final momenta of the two protons, and K is the momentum of the photon in the notation of Sec. VI.

centric system, result in a cross section which is helicity-independent; consequently the cross sections for left- and right-handed polarization of the photon are equal.

VII. RESULTS AND DISCUSSION

The usefulness of p-p-γ in distinguishing among potentials is dependent upon the sensitivity of p-p-γ to the inner region of the nuclear interaction, which is not sufficiently probed by elastic scattering results. To investigate this sensitivity we have compared the results of the hard-core potential of Hamada and Johnston to those of the momentum-dependent one-boson-exchange potential of Bryan and Scott. The latter potential is characterized by the exchange of six

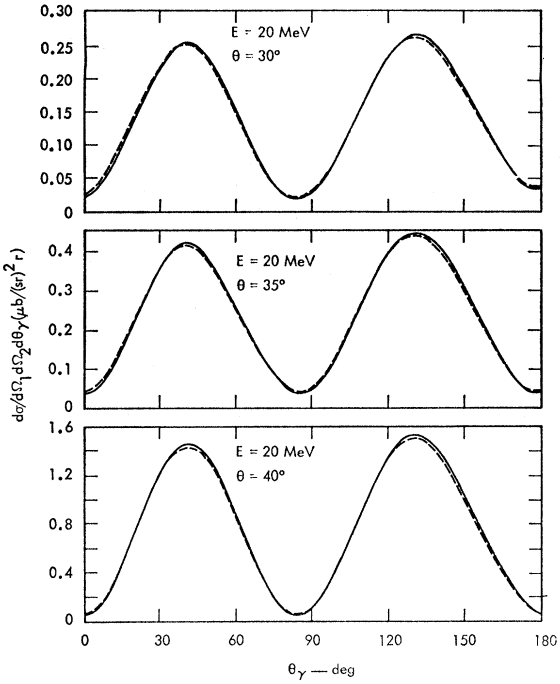

FIG. 4. Coplanar symmetric cross section $d\sigma/d\Omega_1 d\Omega_2 d\theta_\gamma$ calculated with the Hamada-Johnston (dashed curve) and the Bryan-Scott (solid curve) potentials at 20 MeV with coplanar angles of 30°, 35°, and 40°.

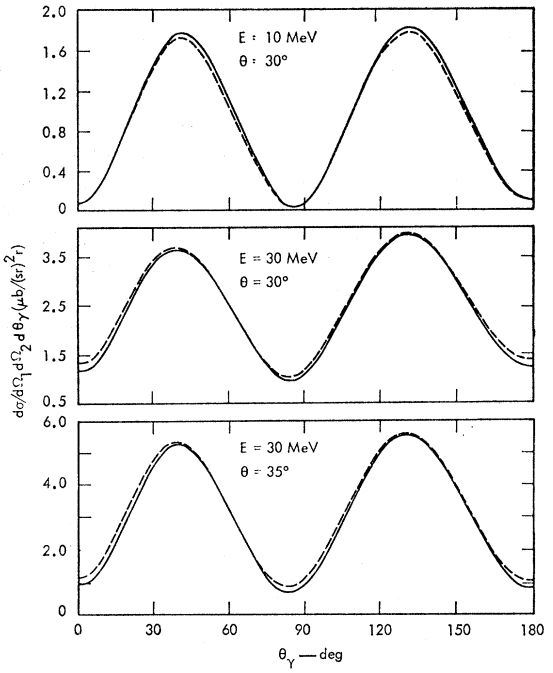

FIG. 3. Coplanar symmetric cross section $d\sigma/d\Omega_1 d\Omega_2 d\theta_\gamma$ calculated with the Hamada-Johnston (dashed curve) and the Bryan-Scott (solid curve) potentials at 10 and 30 MeV with coplanar angles of 30° and 35°.

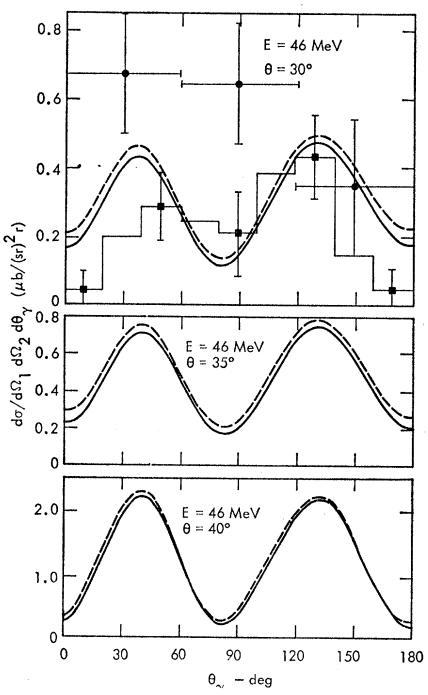

FIG. 5. Coplanar symmetric cross section $d\sigma/d\Omega_1 d\Omega_2 d\theta_\gamma$ calculated with the Hamada-Johnston (dashed curve) and the Bryan-Scott (solid curve) potentials at 46 MeV (30°, 35°, and 40°). Experimental results at 30° are from Refs. 6 (circles) and 9 (squares).

mesons, and has been fitted to S and higher partial waves utilizing a linear Feynman cutoff parameter.

The coplanar symmetric cross section $d\sigma/d\Omega_1 d\Omega_2 d\theta_\gamma$ has been calculated according to Eq. (6.3) for the Bryan-Scott and Hamada-Johnston potentials at representative incident laboratory energies E ranging from 10 to 300 MeV and coplanar symmetric angles $\theta(\theta_1=\theta_2)$ ranging from 20° to 40°. These results include partial-wave contributions of the nuclear matrix elements up to $J\leq 4$ as well as the exact determination of the rescattering contribution. The results for the two potentials are presented in Figs. 3–11; experimental results are included where available. The essentially quadrupole shape of the photon angular distribution is

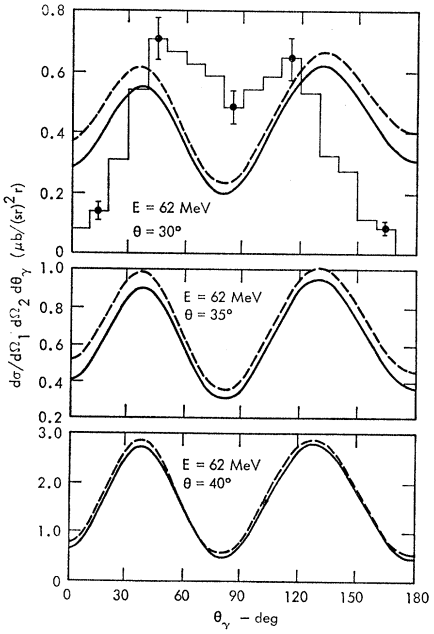

FIG. 6. Coplanar symmetric cross section $d\sigma/d\Omega_1 d\Omega_2 d\theta_\gamma$ calculated with the Hamada-Johnston (dashed curve) and the Bryan-Scott (solid curve) potentials at 62 MeV (30°, 35°, and 40°). The experimental results at 30° are from Ref. 8.

evident in most of the results presented in Figs. 3–11; for coplanar symmetric angles of 40° the quadrupole effect is most pronounced; this is suggested by Nyman[23] to be a model-independent feature. For a fixed incident laboratory energy E and photon angle θ_γ, a decrease in the coplanar symmetric angles θ of the two final protons corresponds to an increase in the photon energy, which in turn corresponds to a decrease in the energy available for the final p-p system. In this sense, then, a decrease in θ corresponds to going farther off the energy shell, and there results, according to Figs. 3–11, a corresponding flattening of the quadrupole effect. In addition, a tendency for forward and backward peaking at 158 and 300 MeV with a decrease of θ to 20° is demonstrated in Fig. 11.

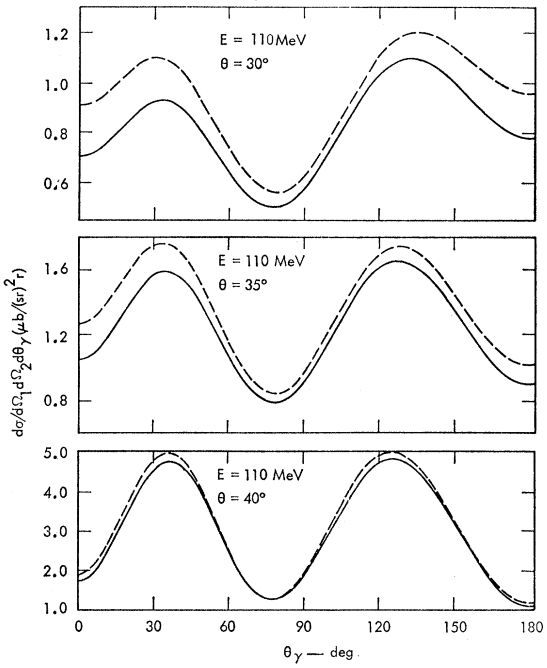

FIG. 7. Coplanar symmetric cross section $d\sigma/d\Omega_1 d\Omega_2 d\theta_\gamma$ calculated with the Hamada-Johnston (dashed curve) and the Bryan-Scott (solid curve) potentials at 110 MeV (30°, 35°, and 40°).

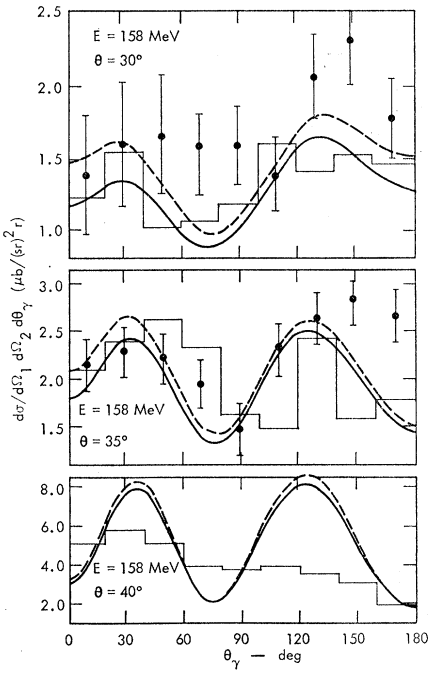

FIG. 8. Coplanar symmetric cross section $d\sigma/d\Omega_1 d\Omega_2 d\theta_\gamma$ calculated with the Hamada-Johnston (dashed curve) and the Bryan-Scott (solid curve) potentials at 158 MeV (30°, 35°, and 40°). The experimental histograms and data points are from Refs. 3 and 4, respectively.

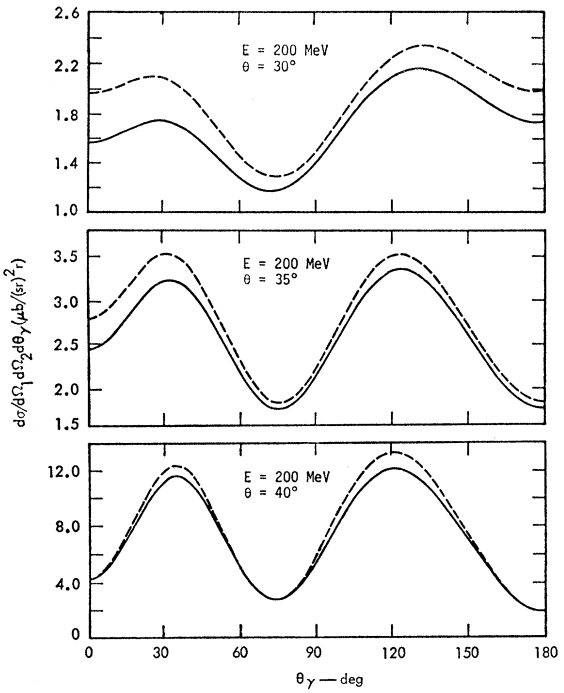

FIG. 9. Coplanar symmetric cross section $d\sigma/d\Omega_1 d\Omega_2 d\theta_\gamma$ calculated with the Hamada-Johnston (dashed curve) and the Bryan-Scott (solid curve) potentials at 200 MeV (30°, 35°, and 40°).

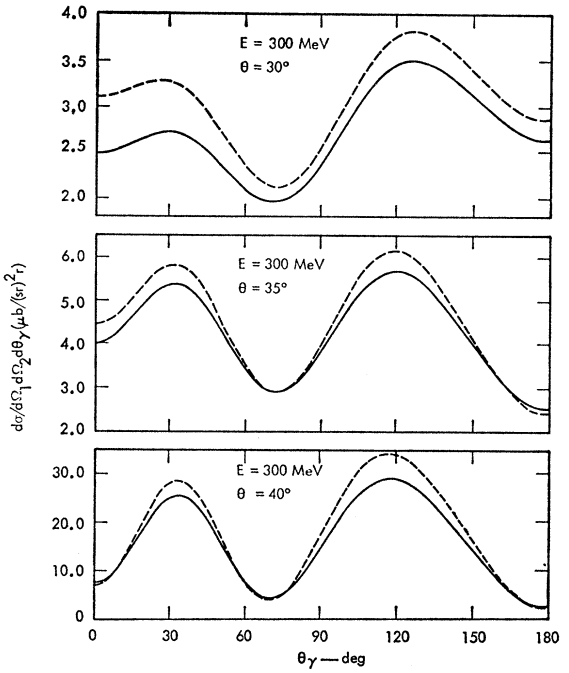

FIG. 10. Coplanar symmetric cross section $d\sigma/d\Omega_1 d\Omega_2 d\theta_\gamma$ calculated with the Hamada-Johnston (dashed curve) and the Bryan-Scott (solid curve) potentials at 300 MeV (30°, 35°, and 40°).

Since a decrease in θ corresponds to going farther off the energy shell, it is not surprising that there is a corresponding increase in the difference of the results of the two potentials, as can be seen by comparing these results at a given energy for a decrease in θ from 40° to 30°. A further separation of the results as calculated with the two potentials is not clearly evidenced at $\theta = 20°$, as shown in Fig. 11. The manner of going off the energy shell described here has a feature that is at

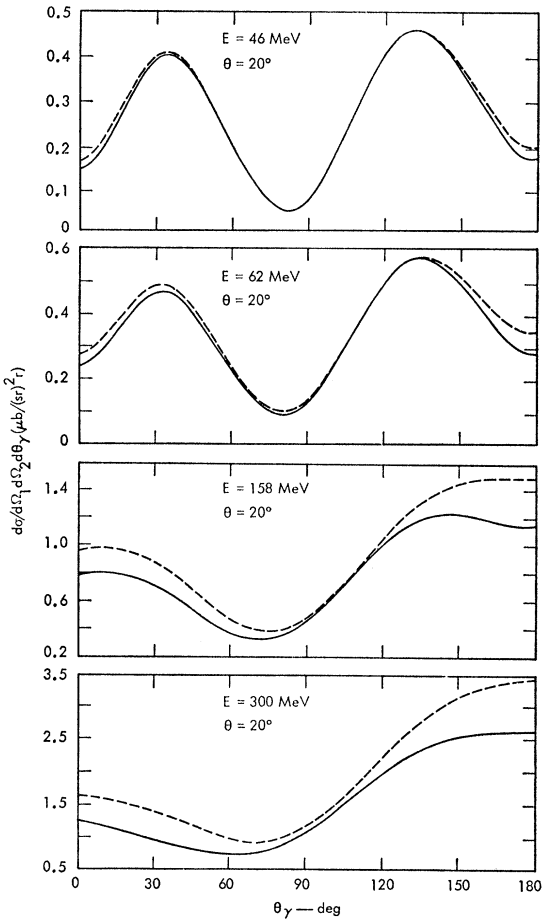

FIG 11. Coplanar symmetric cross section $d\sigma/d\Omega_1 d\Omega_2 d\theta_\gamma$ calculated with the Hamada-Johnston (dashed curve) and the Bryan-Scott (solid curve) potentials at 46, 62, 158, and 300 MeV with coplanar symmetric angles of 20°.

least consistent with this ostensible decrease in sensitivity in the results of the two potentials at 20°. This feature is obviously exhibited only by those nuclear matrix elements that involve the final-state nuclear wave function. Although a decrease in the coplanar symmetric angle puts these matrix elements farther off the energy shell in terms of the relative separation of the energies involved, due to the increase in photon energy, the energy of the final-state nuclear wave function may be sufficiently small to be in a region where

there is little difference in the results of the two potentials. For example, at 158 MeV with coplanar symmetric angles of 20°, the c.m. energy of the p-p system following the emission of the photon is the same as that c.m. energy that would correspond to an incident proton energy of 16 MeV in the laboratory, which is in an energy region in which there is little difference between the results of the two potentials, as seen, for example, in Figs. 3 and 4.

Presented in Fig. 12 is a partial-wave study of the coplanar symmetric cross section $d\sigma/d\Omega_1 d\Omega_2 d\theta_\gamma$ at 158 MeV with symmetric angles of 30°, using the Hamada-Johnston potential. The effect of including the rescattering-term contribution is also presented. The individual curves are labeled according to the p-p states that are included. For example, $J=0$ includes the $^1S_0$ and the $^3P_0$ states, while $J\leq 1$ includes these states plus the $^3P_1$ state. Besides the $^1D_2$ contribution for $J=2$, there is a 2×2 transition matrix corresponding to the mixing of the $^3P_2$ and $^3F_2$ states. To illustrate the size of the off-diagonal contributions to the cross section, we present separately $J\leq 2$ inclusive and $J\leq 2$ ODNI (off-diagonal matrix elements not included). The effect of including the off-diagonal matrix elements for the photon emitted, for example, in the forward direction, is to increase the cross section by a factor greater than 2. The curve labeled $J\leq 3$ shows the effect of including the $^3F_3$ state. The effect of including the $^1G_4$ and the diagonal matrix elements corresponding to the mixing of $^3F_4$ and $^3H_4$, which is given by $J\leq 4$ ODNI, makes little change in the cross section as compared to the $J\leq 3$ results. However, the inclusion of the off-diagonal matrix elements given by $J\leq 4$ shows a decrease in the cross section which amounts to 20% for the photon emitted in the forward direction. The importance of the off-diagonal matrix elements illustrated here suggests (a) the consideration of partial waves with $J\leq 6$ especially at higher energies and (b) the necessity of calculating p-p-γ with a potential for which the effect of the tensor force is included.

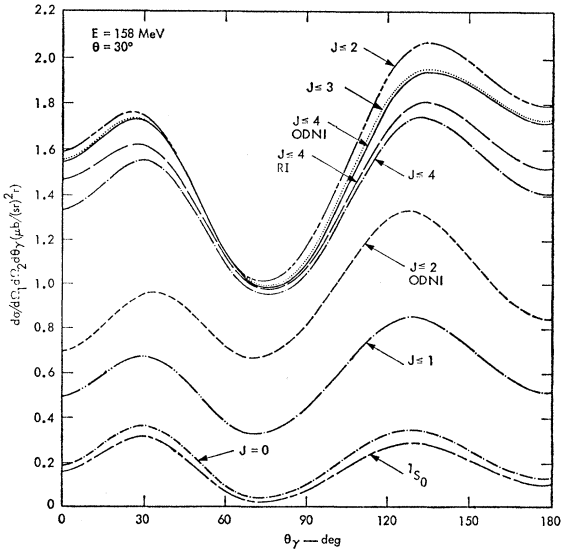

FIG. 12. Partial-wave and rescattering analysis of $d\sigma/d\Omega_1 d\Omega_2 d\theta_\gamma$ calculated with the Hamada-Johnston potential at 158 MeV (30°). Only that curve labeled RI includes rescattering. The total angular momentum of the p-p system includes $J\leq 4$, and for those curves labeled ODNI the off-diagonal matrix elements are not included.

TABLE I. Coplanar symmetric cross section $d\sigma/d\Omega_1 d\Omega_2$ in μb/sr^2 for incident laboratory energy E and coplanar symmetric angles θ as calculated in the present study with the Hamada-Johnston and Bryan-Scott potentials. The experimental results and corresponding references are given in the last two columns.

E (MeV)	θ (deg)	Hamada-Johnston	Bryan-Scott	Experiment	Reference
20	35	1.47	1.47	1.3±0.4	12
30	35	2.05	1.97	1.85±0.25	11
46	30	2.09	1.91	3.3±1.4	6
				1.37±0.29	9
				2.12±0.36	5
46	35	3.19	2.93	3.04±0.44	5
62	30	3.01	2.65	2.27±0.73[a]	8
				2.04±0.24[b]	8
158	30	9.15	8.06	7.8±1.5	3
				(10.6±2.1)	4
	35	13.2	12.3	12.4±2.5	3
				(14.0±2.8)	4
	40	33.0	31.3	23.8±4.8	3
200	30	12.1	10.7	13±2.4	7
	35	17.5	16.4	14±2.7	7
	40	49.1	45.8	29±6.0	7

[a] These results are for the small-aperture geometry of Ref. 8.
[b] These results are for the large-aperture geometry of Ref. 8.

The effect of rescattering as a function of θ_γ is demonstrated explicitly in Fig. 12, where the curve designated as $J\leq 4$, for which rescattering is not included, is compared to the curve labeled $J\leq 4$ RI (rescattering included). The inclusion of rescattering increases the cross section for all photon angles, but it has its greatest effect for the photon emitted in the forward or backward direction, where the increase is 10 and 8%, respectively. The effect of the rescattering contribution on the coplanar symmetric cross section integrated over the photon angular distribution $d\sigma/d\Omega_1 d\Omega_2$ ranges from $\leq 0.2\%$ for energies of the order of 62 MeV and lower to 15% at 300 MeV. As we have seen from $J\leq 4$ RI of Fig. 12, the rescattering contribution to $d\sigma/d\Omega_1 d\Omega_2 d\theta_\gamma$ is dependent upon the photon emission angle θ_γ; it is also dependent upon the coplanar symmetric angles θ. For the results presented in this study, the effect of the rescattering contribution increases for decreasing θ corresponding to a given energy. For the Hamada-Johnston potential calculated at 158 MeV, for example, the effect of including the rescattering contribution in the cross section $d\sigma/d\Omega_1 d\Omega_2$

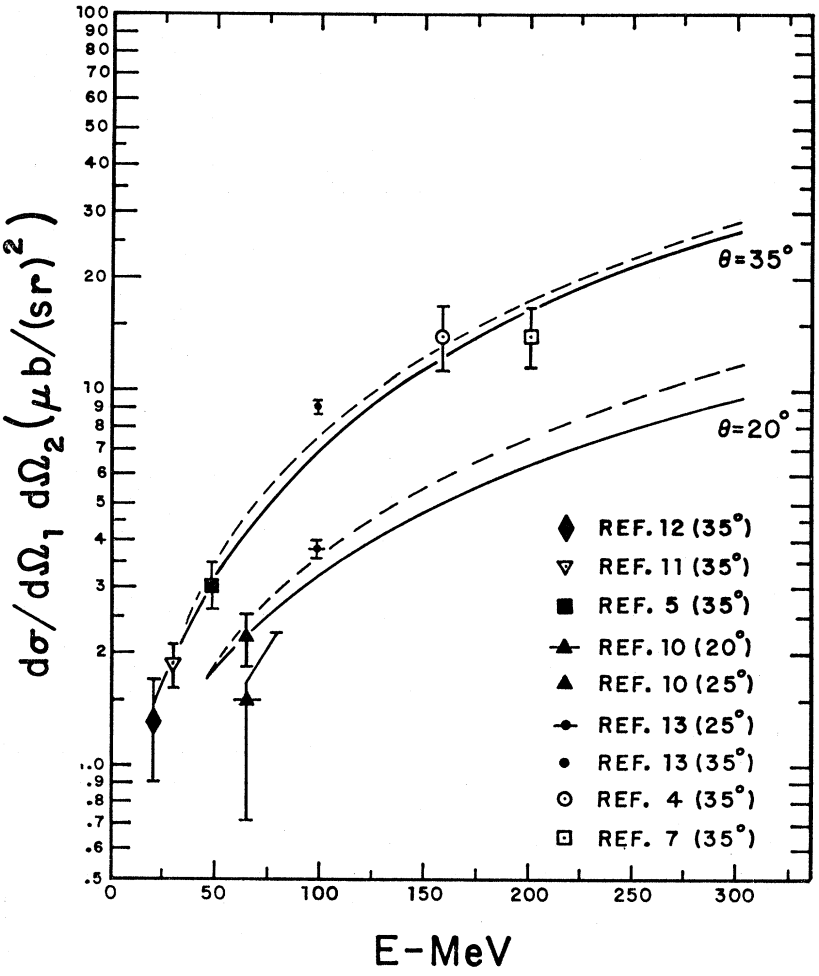

FIG. 13. Integrated cross section $d\sigma/d\Omega_1 d\Omega_2$ calculated with the Hamada-Johnston (dashed curve) and the Bryan-Scott (solid curve) potentials for coplanar symmetric angles of 20° and 35°. Experimental results are included for Refs. 4–13.

for coplanar symmetric angles of 20°, 30°, 35°, and 40° is 5, 4, 3, and 2%, respectively.

The cross section $d\sigma/d\Omega_1 d\Omega_2$, which is integrated over the photon angular distribution, is calculated with the Hamada-Johnston and Bryan-Scott potentials and is compared to experimental results in Table I. The calculations at 46 MeV are compared to the experimental results of Slaus *et al.*,[6] Mason *et al.*,[9] and Warner[5] at 46, 47, and 48 MeV, respectively. It is noteworthy that the experimental results at 47 MeV are somewhat lower than the results at 46 and 48 MeV.

The integrated cross section $d\sigma/d\Omega_1 d\Omega_2$ is presented in Figs. 13 and 14 for the Hamada-Johnston and Bryan-Scott potentials as a function of incident laboratory energy E and coplanar symmetric angles θ of 20°, 30°, 35°, and 40°. Certain experimental results included in Figs. 13 and 14 are not included in Table I, since the calculations have not been performed for precisely the energies and angles involved. These include the experimental results at 65 MeV of Mason *et al.*[10] for θ of 20° and 30°, and those at 99 MeV of Sannes *et al.*[13] for 25°, 30°, 35°, and 40°. An increase in the cross section with θ provides the identification of these experimental results with coplanar angle.

It is seen that for the most part the results of the two potentials as presented in Table I and Figs. 13 and 14 fall within the experimental uncertainties. (These results could be somewhat modified by the inclusion of Coulomb effects, especially at lower energies.) An important source of experimental error is the noncoplanarity correction due to the finite size of the detectors. The noncoplanarity corrections to the results of Halbert *et al.*[8–10] and Sannes *et al.*,[13] as presented here, are based on the Drechsel-Maximon[20] noncoplanar p-p-γ calculations. For the experiments of Halbert *et al.* the results of both potentials fall in the vicinity of the upper limits of the experimental uncertainties. This might be taken as an indication that the Bryan-Scott potential, the results of which are consistently lower than the results of the Hamada-Johnston potential, are favored. On the other hand, the results of Sannes *et al.* tend to favor the Hamada-Johnston potential.

At present, the degree of the experimental uncertainties coupled with the somewhat modest differences

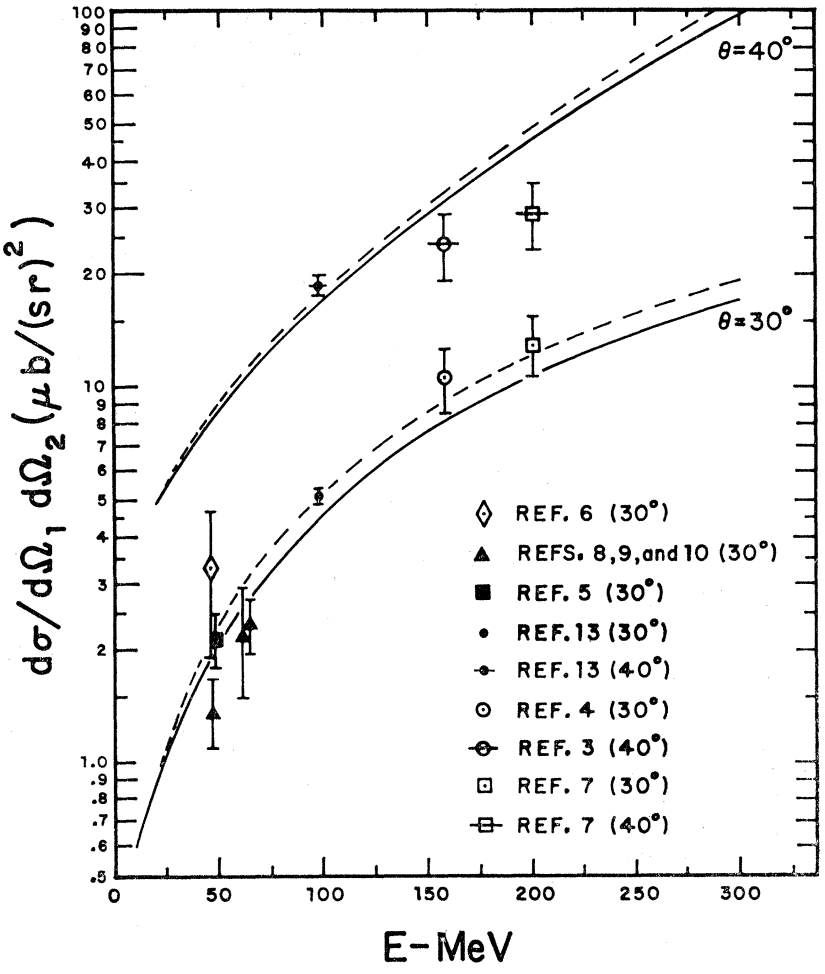

FIG. 14. Integrated cross section $d\sigma/d\Omega_1 d\Omega_2$ calculated with the Hamada-Johnston (dashed curve) and the Bryan-Scott (solid curve) potentials for coplanar symmetric angles of 30° and 40°. Experimental results are included for Refs. 3–13.

in the results associated with the two potentials do not provide a basis for making a clear-cut distinction between the two potentials as to the relative merits of their off-energy-shell behavior as applied to p-p-γ. It is also important to realize that the difference in the p-p-γ results does not exactly represent the difference in the off-energy-shell behavior of the two potentials, since they are not identical on the energy shell. What is needed within the framework of p-p-γ is a more sensitive manner (possibly via polarization studies) of going off the energy shell utilizing potentials that, although fundamentally different, give identical on-shell results. Further refinements in both theory and experiment are needed before any conclusions about the usefulness of p-p-γ as a means of distinguishing among potentials can be obtained.

ACKNOWLEDGMENTS

The author appreciatively acknowledges many useful discussions with Dr. J. Franklin, whose suggestion it was to simplify the off-shell nuclear matrix elements. Special thanks are also due to Dr. R. Bryan and Dr. B. Scott for the use of their potential prior to publication and especially to Dr. R. Bryan for several beneficial discussions regarding the Bryan-Scott potential as related to p-p-γ.